Planta (1997) 202: 435–442

Planta

Atomic force microscopy of cotton fiber cell wall surfaces in air and water: quantitative and qualitative aspects

Thomas C. Pesacreta[1], Lisa C. Carlson[1], Barbara A. Triplett[2]

[1]Microscopy Center, POB 42451, University of Southwestern Louisiana, Lafayette, LA 70504, USA
[2]USDA ARS, Fiber Bioscience Research, POB 19684, New Orleans, LA 70179-0687, USA

Received: 10 December 1996 / Accepted: 29 January 1997

Abstract. Cotton (*Gossypium hirsutum* cv. MD51) fiber cell walls were analyzed with an atomic force microscope to determine the effect of chemical treatments on cell wall organization and topography. Analysis of fibers in either air or water and without any staining or coating produced high-resolution images of cell wall microstructure which could be used for detailed quantitative analysis. Treatment of fibers with 1% H_2O_2 had little effect on surface morphology. Alkali removed much of the cuticle, some primary wall components, and revealed mostly thin-diameter microfibrils. Acidic Updegraff reagent fragmented the fibers, removed much of the cuticle, and revealed mostly thick microfibrils. The surface roughness of fibers treated sequentially with alkali and acid was quantitatively distinguishable from all other fiber types based on the standard deviation of the height data, amplification of surface area, and integration of the scan line data. Analysis of the fractal dimension enabled untreated and peroxide-treated fibers to be clearly distinguished from the other fiber types. Segmentation of the fractal data revealed specific portions of the fractal dimension which were especially useful for defining the size of structures that differentiated fiber types. Areas containing microfibrils could be quantitatively differentiated from non-microfibrillar areas. In water, some alkali-treated fibers had microfibrils that were relatively small in diameter while others appeared to consist of crystalline arrays of smaller fibrils.

Key words: Atomic force microscopy – Cellulose – Cell wall – Fiber (cotton) – *Gossypium* – Microfibril

Introduction

Surface area analysis of biological structure is important to our understanding of function because surface area can affect a variety of mechanical and chemical properties such as friction or adsorption. And yet, a precise measurement of the surface area of cellular structures using microscopy techniques has been hampered by several factors. With the scanning electron microscope, measurement of the surface of dried and coated samples is possible using computer analysis of stereopairs but the process is somewhat problematic and not widely used. The transmission electron microscope can be used to analyze surface structures but the preparation and analysis of serial sections is agonizingly slow. Surface area can also be measured with optical profilers but the poor reflectivity and variable composition of biological samples restrict their use.

Atomic force microscopy is a relatively new technology (Binning et al. 1986) that allows surface topography to be observed and measured in the micrometer (μm) to nanometer (nm) range. Because of important industrial applications (Persch and Born 1993), much work with the atomic force microscope (AFM) has been done with non-biological samples, but the instrument has several capabilities that clearly make it an important instrument for biological research (for reviews, see Radmacher et al. 1992; Hansma and Hoh 1994; Shao et al. 1995).

The attractiveness of the AFM for biologists goes far beyond its resolution capability, which is near or better than that of electron microscopes (Hansma et al. 1988; Kuutti et al. 1995). The AFM is distinguished partly by the fact that it does not require the sample to be coated, stained, or dried. Thus AFM operation is relatively simple, artifacts are reduced, and biological materials can be examined in their native state. Of further relevance is that the AFM offers the investigator a quick and precise method of surface roughness quantification.

The AFM image is derived from the vertical deflection of a tip that is rastered across the sample surface in sub-Angstrom increments. The vertical movement of the

Abbreviations: AFM = atomic force microscope; ANOVA = analysis of variance; FRAC = fractal dimension of the entire surface of each scan; RMS = root mean squared or standard deviation of the height; SAD = surface area deviation; TP = total power or total amplitude derived from integration of the fast Fourier transform of the image

Correspondence to: T.C. Pesacreta; Tel.: 1 (318) 482 5233; Fax: (318) 482 5834; E-mail: tcp9769@usl.edu

AFM tip is monitored by a laser beam that is reflected off the back of the tip onto a photodetector grid. While the vertical resolution of the AFM is in the sub-Angstrom range, lateral resolution is lower because of its dependence on parameters such as tip diameter and sample shape. The highest lateral resolution on biological samples has been by Shao et al. (1995) who imaged 1-nm features on protein molecules.

Our AFM investigation of cotton fibers builds upon earlier analyses that primarily dealt with qualitative aspects of fiber surface morphology (Balls 1923; Farr 1934; Anderson and Kerr 1938; Tripp et al. 1954; Rollins et al. 1965; Westafer and Brown 1976; Ryser 1985). The fiber surface is characterized by an extensive series of low furrows and ridges that are formed by bundles of underlying secondary wall microfibrils arranged in a spiral pattern around the longitudinal axis of the fiber (Tripp and Rollins 1952). Irregularly shaped particulate surface deposits are scattered on the cuticular surface of dried fibers (Goynes et al. 1984). The originally cylindrical shape of the fiber becomes irregularly convoluted and flattened during drying (Duckett 1975) and microfibrillar reversals add to the variation in fiber shape (Patel et al. 1990).

As portions of the cuticle and the microfibrils are removed by chemical treatments, fiber surface roughness becomes modified in ways that influence stainability, luster, and mechanical characteristics such as shear strength (Duckett 1975). Much recent work has focused on methods for evaluating the relationship of surface modification to fiber properties (DeLuca and Thibodeaux 1992; El Mogahzy and Broughton 1993). But the intrinsic variability of the fiber surface has confounded all efforts at direct measurement of roughness until now. In this work we use AFM data to quantitatively and qualitatively describe the elaborate and irregular surfaces of chemically degraded and undegraded fibers in air, and to study microfibril structure in water.

Materials and methods

Instrument. We used a Dimension 3000 AFM (Digital Instruments, Santa Barbara, Calif. USA) mounted on a pneumatic isolation table and covered with an acoustic hood.

Fiber treatments. Seed coat fibers from *Gossypium hirsutum* cv. MD51 were mechanically harvested and ginned. Data were collected either from fibers that had not been treated (these are referred to as A-fibers), or from fibers that had been subjected to one of the following chemical treatments. B-fibers were treated with 1% H_2O_2 at room temperature for 24 h, then rinsed with deionized water and air dried. C-fibers were treated with 6% NaOH at 51 °C for 24 h, rinsed in 1% acetic acid until the rinse solution pH was 7, rinsed with deionized water, rinsed with acetone, and air-dried. E-fibers were treated with Updegraff reagent (acetic acid/H_2O/HNO_3, 8:2:1, by vol.) for 30 min at 100 °C, rinsed with deionized water, rinsed with acetone, and air-dried. F-fibers were treated sequentially with NaOH as outlined for the C-fibers, and then treated with Updegraff reagent as outlined for the E-fibers.

Observation conditions. Typically, long fibers were shaped like irregularly twisted and partially flattened tubes. Portions of the fiber surface that were lying roughly parallel to the plane of the scan were used for data collection. A scan size of 2.5 μm × 2.5 μm was chosen for most work because it represented a significant portion of the fiber surface (the diameter of each fiber is approx. 15 μm), allowed us to clearly see microfibrils, and greatly reduced the chances of the tip falling off the fiber and onto the adjacent adhesive during a scan.

For most of our work, fibers were imaged in the tapping mode in air, at room temperature. In this mode, changes in the amplitude of the oscillating tip are used to detect sample height. To eliminate tip-size-variabiliy artifacts a single silicon tip was used to collect all of the air tapping images presented here. A format of 512 × 512 pixels was used for all the micrographs shown here except for Fig. 7 which was collected at 256 × 256 pixels. For quantitative data collection, several tips were used and a format of 256 × 256 pixels was used to minimize data storage requirements and speed the collection and analysis.

For imaging in the air tapping mode, fibers were placed onto stubs that were covered either with sticky tabs or Tempfix. Fibers that had not been fragmented during chemical treatment (i.e. fibers A, B, and C) could be forced into tabs at easily observable points along their length with forceps. Because E- and F-fibers fragmented into short pieces during chemical treatment, they were either pushed into the tab with aluminum foil or dropped onto a Tempfix-coated disc which was then heated to 40 °C for a few seconds so that the fibers adhered to it. For imaging in the liquid tapping mode, fibers were pressed onto an adhesive tab using the peel-off side of the tab. Liquid tapping was done with an etched, 100-μm-long silicon nitride tip in deionized water.

Data presentation and analysis. For image presentation only, the data were flattened (setting 2 or 3) to remove scan-line offsets and then contrast-enhanced (setting 9, size 2) so that the details were clear. The flattening procedure reduced the topographic amplitude. Figure 7 was also low-pass-filtered to remove high-frequency noise. In Figs. 1–8 the longitudinal axis of each fiber is from left to right.

For data analysis, 32 images of each fiber type were used. This set size was empirically established by statistically analyzing the data with Statview (Abacus Concepts; Berkeley, Calif., USA) as sampling was in progress to determine when differences became clearly evident between some of the fiber treatment means at the 95% confidence level. The surface roughness of each image was analyzed with Dimension 3000 software that allowed us to quantify the following parameters: RMS, the root mean squared or standard deviation of the height (Z) data; SAD, the surface area deviation or the increase in total surface area within the scanned area compared to a flat surface having the same horizontal dimensions; TP, the total power or total amplitude derived from an integration of the fast Fourier transform of the image; and FRAC, the fractal dimension of the entire surface of each scan. The fractal dimension data were segmented for further analysis by visually inspecting many fractal curves and then empirically dividing the abscissa into three segments that contained approximately linear portions of the fractal curves.

Results

Morphology

Untreated fibers. A-fibers were covered by a cuticle. On some portions of the surface, numerous furrows and ridges (Fig. 1) spiraled around the longitudinal axis of the fiber. Other areas were relatively flat. Particulate/plaque-like structures were visible on the surface of the cuticle. The number, shape and size of such structures varied considerably along the length of each fiber.

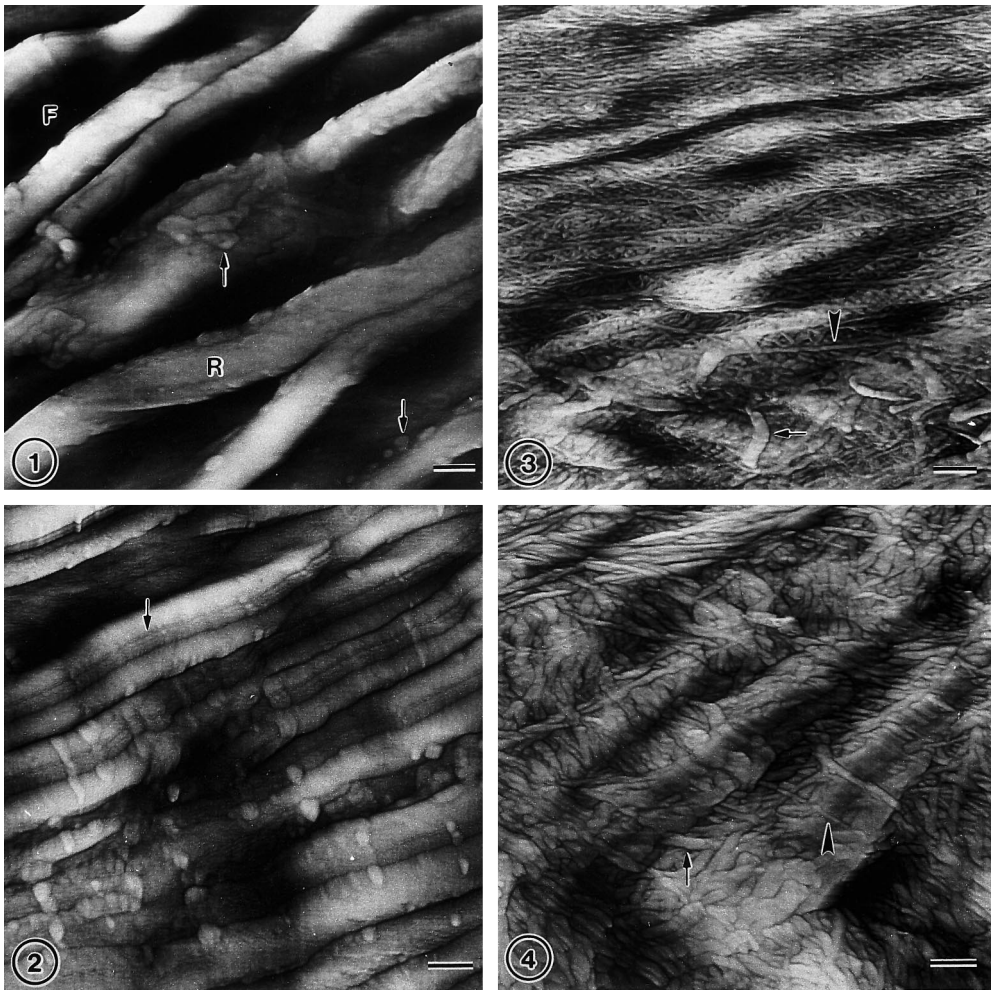

Fig. 1. A-fiber of cotton in air. *Arrows* indicate plaque-like particulate material on cuticle surface. R, ridge; F, furrow. × 39 000; bar = 200 nm

Fig. 2. B-fiber in air. Note apparent collapsed ridge (*arrow*) and high number of particulate materials. × 39 000; bar = 200 nm

Fig. 3. C-fiber in air. Small-diameter microfibrils (*arrowhead*) occur frequently but some large-diameter microfibrils are present (*arrow*). × 39 000; bar = 200 nm

Fig. 4. E-fiber in air. Large-diameter microfibrils (*arrow*) occur frequently but some small-diameter microfibrils are present (*arrowhead*). × 39 000; bar = 200 nm

Peroxide-treated fibers. The surface of B-fibers (Fig. 2) was similar to that of the A-fibers. This was to be expected because peroxide treatment is typically used to modify cell wall carbohydrates rather than cuticular waxes. Again, the range of morphological variation was high and the surface of some portions of B-fibers resembled Fig. 1.

Alkali-treated fibers. The surface of C-fibers contained areas that were markedly different from both the A- and B-fiber types. Frequently, numerous microfibrillar structures were present (Fig. 3). The diameter of these microfibrils was difficult to measure in all cases because of the interlaced structure of the wall components. In cases where clear measurements could be made the microfibril diameters ranged from 25 to 75 nm and they appeared to comprise two groups. One group had diameters of 25–40 nm and heights < 10 nm. The other had diameters of 40–75 nm and heights ranging between 10 and 20 nm. The size and organization of the smaller microfibrils resembles previously published images of cotton primary wall microfibrils (Trip and Rollins 1952; Arthur 1990). The larger microfibrils may be from the secondary wall which, as a result of chemical degradation, is no longer covered by the primary wall in some areas. Non-fibrillar structures similar to those seen on A- and B-fibers were frequently observed on the surface of C-fibers. In some cases such non-fibrillar structures covered the entire scan area, implying that removal of the cuticle was far from complete.

Acid-treated fibers. E-fibers (Fig. 4) were similar to C-fibers in that they had many microfibrils on their surfaces. But, the microfibrils structures on E-fibers were almost exclusively of the > 10 nm height/40–75 nm diameter type. Again, as for C-fibers, substantial numbers of non-fibrillar structures occurred on some areas of the surface.

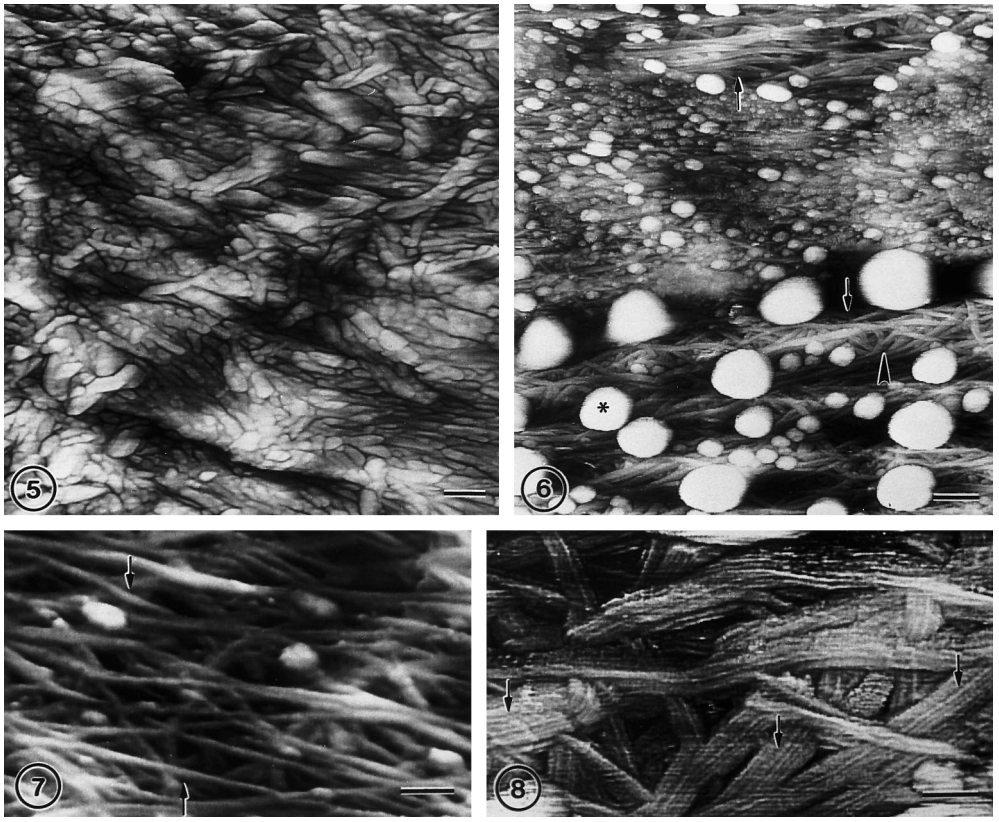

Fig. 5. F-fiber in air. Large-diameter microfibrils cover a surface that is almost devoid of furrows and ridges. × 39 000; bar = 200 nm

Fig. 6. C-fiber in water. This image shows the mix of residual cuticular and microfibrillar (*arrows*) materials that are frequently observed on the surface of this fiber type. The large round structures (*asterisk*) are presumably remnants of the cuticle or some other portion of the fiber that have become adsorbed onto the surface. × 39 000; bar = 200 nm

Fig. 7. C-fiber in water. This image shows a mass of individual microfibrils distributed in a web-like pattern that resembles that known for the primary wall. *Arrows* indicate some of the microfibrils that are < 25 nm in diameter. × 99 000; bar = 100 nm

Fig. 8. C-fiber in water. High magnification of the area indicated by the arrowhead in Fig. 6. Portions of the microfibrils are striated (*arrows*). × 168 500; bar = 59 nm

Alkali/acid-treated fibers. The surface of F-fibers (Fig. 5) was almost exclusively composed of microfibrils that were similar to those seen on E-fibers. Non-fibrillar structures were almost never observed on the surface of F-fibers, implying that the cuticle was no longer present. Few ridges and furrows were observed.

Liquid tapping. Numerous difficulties initially prevented imaging with this very recently developed mode. Tempfix was not a suitable adhesive. It was almost impossible to engage the tip on either the fiber surface or on the surface of the Tempfix so that the trace and retrace lines coincided. But, the adjacent metal surface of the disc could easily be reliably engaged. Fibers clamped to a bare metal surface could not be easily engaged, but fibers that were firmly pressed onto adhesive tabs could be. We concluded from these attempts that fibers had to be firmly attached to a relatively rigid surface in order to provide an environment that was appropriate for the maintenance of both hydrostatic pressure and sample immobility.

The morphology of C-fibers imaged in water (Figs. 6–8) was in many ways similar to those seen with tapping in air. Fibers of approximately the same two diameter ranges were observed although the small-diameter microfibrils sometimes were in the < 25-nm range (Fig. 7). To strengthen the conclusion that microfibrils seen with the liquid tapping mode had relatively small apparent diameters, we sequentially examined a specific portion of one fiber with both modes and confirmed these observations. Also, use of liquid tapping tips from different wafers did not change the diameter values.

At the highest magnifications used (Fig. 8) it became obvious that the surface of many of the microfibrils was striated. The diameter of these surface striations was in the 5- to 7-nm range. The direction of scanning did not influence our ability to detect the presence of the striations, making it unlikely that they were tip-shape artifacts.

Quantitative surface roughness

Data from 2.5 μm × 2.5 μm *scans*. Statistical analysis of the data from 32 scans of each fiber type in air provided a method for clearly distinguishing each fiber type from

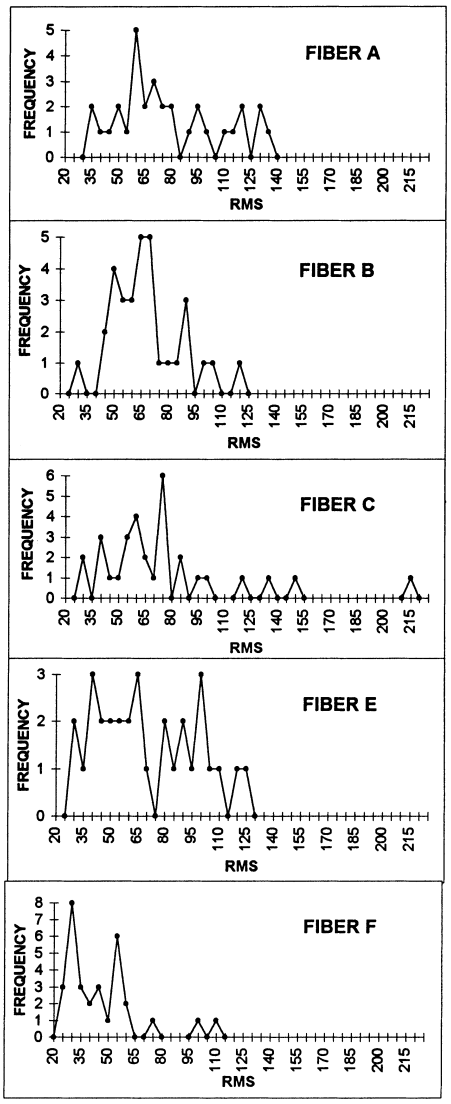

Fig. 9. Distribution of RMS values in the raw data from each treatment

the others without having to exclude any outliers. Figure 9 shows the frequency of the RMS values for each fiber type. Most of the values are from different fibers. The fibers are more than several millimeters long and we found that the RMS varied greatly between points that were separated by several hundred micrometers. For C- and F-fibers a few low-frequency, high-RMS outliers contributed to the substantial variation that we encountered, and probably are a reflection of the intrinsic morphological diversity of fibers.

The means and 95% confidence intervals for each treatment are shown in Table 1. From these data and from the analysis of variance (ANOVA; Table 2) it is evident that chemical treatment does have a significant effect on surface roughness. Comparison of the different treatments shows that F-fibers can be separated from all the other treatments by using the TP, RMS, and SAD parameters, although TP is, in a relative sense, the least powerful parameter. These results indicate that the F-fibers have smaller features. The same conclusion was initially reached by comparing the data for F-fibers in Fig. 9 with the other treatment data.

In contrast with the above parameters, the average fractal dimension of A- and B-fibers was significantly lower than for C-, E-, and F-fibers (Table 2). To determine the size of the structural features that are the most useful for differentiating fiber types, we segmented the fractal data (Table 3). The ANOVA analysis indicated that structures affecting the intermediate fractal range between 9.0×10^{-2} μm^2 to 1.6×10^{-3} μm^2

Table 1. Raw data from 6.25-μm^2 scans was analyzed without modification. Numbers in brackets indicate 95% confidence interval

	TP	RMS	SAD	FRAC
A	11240 [3744]	78.94 [10.49]	14.29 [2.55]	2.120 [0.014]
B	8636 [2072]	70.66 [6.99]	16.13 [2.97]	2.118 [0.011]
C	13080 [6448]	77.30 [13.61]	13.61 [2.30]	2.156 [0.024]
E	9240 [2897]	72.91 [9.82]	15.64 [2.86]	2.152 [0.016]
F	3556 [1619]	42.03 [7.42]	8.35 [1.66]	2.162 [0.019]

Table 2. Fiber comparisons using the Fisher's PLSD test run on ANOVAs of raw data from the 6.25-μm^2 scans. Asterisks signify those fiber comparisons that have statistically significant *P*-values

Fiber Comparisons	TP	RMS	SAD	FRAC
Large A, Large B	0.3015	0.1881	0.4118	0.8583
Large A, Large C	0.4953	0.7273	0.5348	0.0029*
Large A, Large E	0.4232	0.3227	0.5881	0.0099*
Large A, Large F	0.0031*	< 0.0001*	0.0004*	0.0007*
Large B, Large C	0.0896	0.3360	0.1536	0.0018*
Large B, Large E	0.8169	0.7438	0.7813	0.0063*
Large B, Large F	0.0528	< 0.0001*	< 0.0001*	< 0.0004*
Large C, Large E	0.1422	0.5245	0.2495	0.6841
Large C, Large F	0.0003*	< 0.0001*	0.0033*	0.6672
Large E, Large F	0.0305*	< 0.0001*	< 0.0001*	0.4031

Table 3. Fractal comparisons using the Fisher's PLSD test run on ANOVAs of raw data from the 6.25-μm^2 scans. Small indicates features below 1.6×10^{-3} μm^2; Intermediate indicates features from 1.6×10^{-2} μm^2 to 9.8×10^{-2} μm^2; Large indicates features larger than 9.8×10^{-2} μm^2. Asterisks signify those fiber comparisons that have statistically significant *P*-values

Fractal Comparisons	Small	Intermediate	Large
A, B	0.0593	0.5981	0.5260
A, C	0.0096*	< 0.0001*	0.7353
A, E	0.6052	0.0016*	0.0586
A, F	0.4456	< 0.0001*	0.8445
B, C	0.4588	< 0.0001*	0.3193
B, E	0.0148*	0.0002*	0.0102*
B, F	0.2522	< 0.0001*	0.3977
C, E	0.0017*	0.1195	0.1097
C, F	0.0612	0.2870	0.8863
E, F	0.1939	0.0099*	0.8410

(i.e. lateral dimensions within the range of 310 nm × 310 nm to 40 nm × 40 nm) were consistently useful for differentiating both A- and B-fibers from C-, E-, and F-fibers. However, the larger and smaller ranges were less useful.

Data from small scans that are subsets of the 2.5 μm × 2.5 μm *scans*. We were surprised that, for TP, RMS and SAD, the A- and B-fibers were similar to the C- and E-fiber types (Tables 1, 2) which clearly had much more fibrillar surface (Figs. 1–4). In an effort to determine if it was possible to use these parameters to differentiate each fiber type we initiated an analysis of subjectively selected 244 nm × 244 nm (0.06 μm^2) areas that were extracted from the original 2.5 μm × 2.5 μm (6.25 μm^2) scans. This size was used because it allowed us to easily sample areas that contained exclusively microfibrils (in the case of C-, E-, and F-fibers) or particulate materials (in the case of A- and B-fibers) on relatively flat surfaces. Each area was extracted with the "Zoom and Planefit" program, and then further treated with a zero-order flatten program to remove artifactual scan-line offsets.

Table 4 shows the means and 95% confidence intervals of the RMS values for the small scans. Here the TP, RMS, and SAD values for A- and B-fibers are relatively low. The ANOVA analysis of the data (Table 5) shows that statistically significant variation occurs between either A- or B-fibers and the other fiber types. This conclusion indicates that the irregular, particulate structures can be quantitatively differentiated from the microfibrillar areas. It is probable that had we included non-particulate, smooth areas of A- and B-fibers in the "small scan" analysis, we would have found even greater differences compared with the data from C-, E-, and F-fibers. The comparative conclusions here are much different from those in Table 2. This analysis strongly suggests that, for the 6.25-μm^2 scans, the parameters TP, RMS, and SAD are dominated by the effect of topographic features that were not present in the 0.06-μm^2 scans as we prepared them for analysis (i.e. after plane fitting and flattening). Since the furrows and ridges caused by bundles of secondary microfibrils were not present in the small scans, it is likely that they are the features that dominate the data for the 6.25-μm^2 scans.

Table 4. 0.06-μm^2 scans. Raw data extracted by Zoom function from 6.25-μm^2 scans. Zoomed area was plane-fitted and flattened (zero order) prior to analysis. Numbers in brackets indicate 95% confidence interval

Fiber type	TP	RMS	SAD	FRAC
A	23.49 [5.86]	4.64 [0.53]	2.99 [0.37]	2.069 [0.017]
B	13.78 [3.18]	3.57 [0.45]	2.26 [0.59]	2.073 [0.018]
C	36.17 [8.21]	5.86 [0.65]	6.39 [1.74]	2.091 [0.020]
E	35.29 [6.67]	5.73 [0.57]	4.28 [1.26]	2.060 [0.011]
F	30.55 [6.68]	5.31 [0.54]	4.12 [0.56]	2.060 [0.012]

Table 5. Fiber comparisons using the Fisher's PLSD test run on ANOVAs of raw data from the 0.06-μm^2 scans. Asterisks signify those fiber comparisons that have statistically significant *P*-values

Fiber Comparisons	TP	RMS	SAD	FRAC
Small A, Small B	0.0317*	0.0070*	0.2130	0.7286
Small A, Small C	0.0067*	0.0028*	< 0.0001*	0.0535
Small A, Small E	0.0052*	0.0030*	0.0741	0.3684
Small A, Small F	0.0882	0.1624	0.0375*	0.3418
Small B, Small C	< 0.0001*	< 0.0001*	< 0.0001*	0.1347
Small B, Small E	< 0.0001*	< 0.0001*	0.0044*	0.2415
Small B, Small F	0.0003*	< 0.0001*	0.0018*	0.2227*
Small C, Small E	0.8487	0.7495	< 0.0001*	0.0069*
Small C, Small F	0.2237	0.0753	0.0002*	0.0059*
Small E, Small F	0.2556	0.1054	0.7771	0.9656

Discussion

Each new microscopy technique must extend our analytical capabilities if it is to become a significant research tool. Our quantitative data from fibers imaged in air provide the first direct statistical analysis of single-fiber roughness. It is remarkable that, for the 6.25-μm^2 scans, RMS, TP and SAD are difficult to correlate with the size and number of microfibrils observed on the fiber surface. As Tables 1 and 2 show, E, the fiber type that is partially surfaced with large-diameter fibrils, is characterized by TP, RMS, and SAD values comparable to C, the fiber type with small microfibrils. Also, the partial removal of the cuticle and the concomitant exposure of microfibrils on C- and E-fibers did not significantly change their roughness values (except for the fractal) from those of A- and B-fibers. Nevertheless, the importance of the cuticle to shape parameters is indicated by the fact that the fractals for A- and B-fibers are significantly lower than those of all of the other fiber types.

At the smallest level of structure that we studied, the so-called small scans, we were able to detect variations in roughness that were very different from those found in the large-scan data. The small-scan data show that the large and small microfibrillar areas were quantitatively different from each other and from the nonfibrillar areas. Given the multiplicity of forms present on the fiber surfaces, perhaps it is not surprising that we had to reduce the size of the areas that were analyzed in order to differentiate the surfaces of A- and B-fibers from the others. This conclusion correlates well with our difficulty in finding significant differences in the small fractal segments (Table 3). The unexpected significant difference observed between A- and B-fibers in Table 5 may be due to morphological changes caused by the extraction of a wide range of chemical species from the B-fibers during treatment (Domelsmith et al. 1986). Taken as a whole the small-scan data show that relatively small features are of great utility for the quantitative differentiation of biological surfaces.

While the RMS, TP, and SAD data provided useful information, the fractal dimension analysis substantially extended our understanding of surface roughness. For

example, the large-scan RMS data of F-fibers showed a relatively smooth surface but the high fractal dimension showed that the densely microfibrillar F-fibers have a relatively complex surface.

By segmenting the fractal data (Table 3), the importance of morphological structures within the intermediate range became obvious. This segment of the fractal data is completely consistent with the A, B, C, E, F dichotomy shown by the unsegmented fractal data (Table 2). It also includes the transverse dimensions of many of the secondary microfibril bundles in A-, B-, C-, and E-fibers. Surprisingly, in the small range, fractals detect a significant difference between C- and E-fibers. This must reflect a difference between the 25- to 40-nm microfibrils and the 40- to 75-nm microfibrils. This agrees with the small-scan fractal C/E comparison in Table 5 and again indicates that the fractal dimension can play a useful role in the analysis of the cotton fiber surface.

To briefly sum our quantitative results, several factors are consistent with the hypothesis that ridges and furrows due to bundles of secondary microfibrils have a major effect on roughness. First, they affect the intermediate fractal segment which is the one that is the most consistent with the total fractal data. Secondly, the small-scan data show that when the topographic effect of the ridges and furrows is deleted, the microfibrillar and other small structures on the surface become important to the analysis of roughness. Thirdly, the partial removal of the cuticle does not suffice to differentiate A- and B-fibers from C- and D-fibers.

Hanley et al. (1992) reported that AFM data grossly overstate the diameter of cellulose microfibrils. However, they used the contact mode of operation which we found to be inferior for imaging microfibrils. The range of values that we observed for the microfibril diameter of dry primary wall fibers (25–40 nm) agrees with the transmission electron microscopy study of Tripp and Rollins (1952) and Tripp et al. (1954) who reported that primary wall microfibrils from crude extracts of cotton fibers were in the 10- to 40-nm range. Boylston and Hebert (1995) reported that cotton secondary wall fibrils are approximately twice the thickness of those from primary walls, strengthening the conclusion that the larger microfibrils we observed were secondary.

The liquid tapping images shown here are the highest resolution images of cotton microfibrils in water to date. The detail in these images is at least equal to that of contemporary images of chemically extracted plant primary walls observed with freeze-etch, electron microscopy techniques where microfibril diameters in the 16- to 20-nm range were observed in onion bulb walls (McCann et al. 1990). The 5- to 7-nm striations that we observed on the surface of fibers in water may be crystalline bundles of glucose chains that exist within each microfibril and are called elementary fibrils by some investigators (for a review, see Krassig 1993). Numerous investigations (Krassig 1993) have reported that the diameter of elementary fibrils is in the 1.5 to 3.8-nm range and Boylston and Hebert (1995) have reported a figure of 3–4 nm for cotton "fibrils". Quite possibly, the well-known phenomenon of "tip broadening" slightly increased the apparent diameter that we observed to 5–7 nm. Also, our alkali treatment could have altered microfibrillar sub-structure. These results extend the usefulness of the AFM to the study of intra-microfibrillar organization, a subject which is closely related to the mechanical characteristics of cellulose.

The liquid tapping images are also important because they are the first, to our knowledge, of cotton microfibrils observed in water. In fact, high-resolution images of biological materials in water are rare. Previous AFM researchers have used either partially dehydrated samples (Hansma et al. 1992; Radmacher et al. 1995) or have observed the surface of hydrated samples that have been exposed to the air (Kirby et al. 1995a) to view biological samples in solution.

As to why the apparent microfibril diameter should decrease in water, there are several possibilities. In an aqueous environment, microfibrils may not be as closely associated with each other as they would be in an air-dried state. This may allow the AFM tip to better detect their boundaries. Also, it is known that cellulose microfibrils can be highly asymmetric in cross-section (Krassig 1993) or twisted (Willison and Abeysekera 1985) and so the lower diameter values may simply be a consequence of the orientation of the microfibril to the tip. Other studies by Fritz et al. (1995) and Kirby et al. (1995b) of microtubules and xanthan molecules, respectively, have shown that the AFM can accurately detect the diameter of biological structures that are similar in size to microfibrils.

References

Anderson DB, Kerr T (1938) Growth and structure of cotton fibre. Ind Eng Chem 30: 48–54

Arthur JC Jr (1990) Cotton. In: Kroschwitz JI (ed) Polymers: Fibers and textiles, a compendium. Wiley, New York, pp 118–141

Balls WL (1923) The determiners of cellulose structure as seen in the cell-wall of cotton hairs. Proc R Soc London Ser B 95: 72–89

Binning G, Quate CF, Gerber CH (1986) Atomic force microscope. Phys Rev Lett 56: 930–933

Boylston EK, Hebert JJ (1995) The primary wall of cotton fibers. Tex Res J 65: 429–431

DeLuca LB, Thibodeaux DP (1992) The relative importance of fiber friction and torsional and bending rigidities in cotton sliver, roving and yarn. Tex Res J 62: 192–196

Domelsmith LN, Berni RJ, Cocke JB (1986) Chemical analyses of washed, bleached and scoured and bleached cotton fiber. Tex Res J 56: 14–21

Duckett KE (1975) Surface properties of cotton fibers. In: Shick MJ (ed) Surface characteristics of fibers and textiles. Dekker, New York, pp 67–108

El Mogahzy YE, Broughton RM (1993) A new approach for evaluating the frictional behavior of cotton fibers. Tex Res J 63: 465–475

Farr WK (1934) Cotton fibers I. Origin and early states of elongation. Contrib Boyce Thompson Inst 6: 458–471

Fritz M, Radmacher M, Cleveland JP, Allerma MW, Stewart RJ, Janmey P, Schmidt CF, Hansma PK (1995) Imaging globular and filamentous proteins in physiological buffer solutions with tapping mode atomic force microscopy. Langmuir 11: 3529–3535

Goynes WR, Carra JH, Berni RJ (1984) Changes in cotton fiber surfaces due to washing. Tex Res J 54: 242–247
Hanley SJ, Giasson J, Revol J-F, Gray DG (1992) Atomic force microscopy of cellulose microfibrils: comparison with transmission electron microscopy. Polymer 33: 4639–4632
Hansma HG, Hoh JH (1994) Biomolecular imaging with the atomic force microscope. Annu Rev Biophys Chem 23: 115–139
Hansma PK, Elings VB, Marti O, Bracker CE (1988) Scanning tunneling microscopy and atomic force microscopy: application to biology and technology. Science 242: 209–216
Hansma Hg, Vesenka J, Siegerist C, Kelderman G, Morrett H, Sinsheimer RL, Elings V, Bustamente C, Hansma PK (1992) Reproducible imaging and dissection of plasmid DNA under liquid with the atomic force microscope. Science 256: 1180–1184
Kirby AR, Gunning AP, Morris VJ (1995a) Atomic force microscopy in food research: a new technique comes of age. Trends Food Sci Technol 6: 359–365
Kirby AR, Gunning AP, Morris VJ (1995b) Imaging xanthan gums by atomic force microscopy. Carbohydr Res 267: 161–166
Krassig HA (1993) Cellulose structure, accessibility, and reactivity. Gordon and Breach Science Publishers, USA
Kuutti L, Peltonen J, Pere J, Teleman O (1995) Identification and surface structure of crystalline cellulose studied by atomic force microscopy. J Microsc 178: 1–6
McCann MC, Wells B, Roberts K (1990) Direct visualization of crosslinks in the primary plant cell wall. J Cell Sci 96: 323–334
Patel GS, Iyer PB, Sreenivasan S, Iyer KRI (1990) Reversal in cotton: a study with scanning electron microscopy. Tex Res J 60: 771–774
Persch G, Born C. (1993) Applications of scanning probe microscopies in technology and manufacturing. Scanning (USA) 15: 283–290
Radmacher M, Tillman RW, Fritz M, Gaub HE (1992) From molecules to cells: imaging soft samples with the atomic force microscope. Science 257: 1900–1905
Radmacher M, Fritz M, Hansma PK (1995) Imaging soft samples with the atomic force microscope – gelatin in water and propanol. Biophys J 69: 264–270
Rollins ML, Moore AT, Goynes WR, Carra JH, de Gruy IV (1965) Electron microscopy of chemically modified cotton. Am Dyestuff Rep 5: 36–48
Ryser U (1985) Cell wall biosynthesis in differentiating cotton fibres. Eur J Cell Biol 39: 236–256
Shao Z, Yang J, Somlyo AP (1995) Biological atomic force microscopy: from microns to nanometers and beyond. Annu Rev Cell Dev Biol 11: 241–265
Tripp V, Rollins ML (1952) Morphology and chemical composition of certain components of cotton fiber cell wall. Anal Chem 24: 1721–1728
Tripp VW, Moore AT, Rollins ML (1954) A microscopical study of the effects of some typical chemical environments on the primary wall of the cotton fiber. Tex Res J 11: 956–970
Westafer J, Brown RM Jr. (1976) Electron microscopy of the cotton fibre: new observations on cell wall formation. Cytobios 15: 111–138
Willison JMH, Abeysekera RM (1985) On the form and arrangement of cell wall microfibrils. In: Robards AW (ed) Botanical microscopy 1985. Oxford Univ. Press, Oxford, pp 181–204